



# A high-TOC shale in a low productivity world: The late Mesoproterozoic Arctic Bay Formation, Nunavut

Malcolm S.W. Hodgskiss<sup>a,\*</sup>, Pierre Sansjofre<sup>b</sup>, Marcus Kunzmann<sup>c</sup>, Erik A. Sperling<sup>a</sup>, Devon B. Cole<sup>d</sup>, Peter W. Crockford<sup>e,f</sup>, Timothy M. Gibson<sup>g</sup>, Galen P. Halverson<sup>h</sup>

<sup>a</sup> Department of Geological Sciences, Stanford University, Stanford, CA, USA

<sup>b</sup> Muséum National d'Histoire Naturelle, Sorbonne Université, CNRS UMR 7590, Institut de Minéralogie, de Physique des Matériaux et de Cosmochimie, Paris, France

<sup>c</sup> CSIRO Mineral Resources, Australian Resources Research Centre, Kensington, WA, Australia

<sup>d</sup> School of Earth and Atmospheric Sciences, Georgia Institute of Technology, Atlanta, GA, USA

<sup>e</sup> Department of Earth and Planetary Sciences, Weizmann Institute of Science, Rehovot, Israel

<sup>f</sup> Department of Geoscience, Princeton University, Princeton, NJ, USA

<sup>g</sup> Department of Earth Sciences, Dartmouth College, Hanover, NH, USA

<sup>h</sup> Department of Earth & Planetary Sciences, McGill University, Montréal, QC, Canada

## ARTICLE INFO

### Article history:

Received 18 February 2020

Received in revised form 19 May 2020

Accepted 1 June 2020

Available online xxxx

Editor: L. Derry

### Keywords:

Mesoproterozoic

TOC

shale

sulphurisation

Arctic Bay Formation

redox

## ABSTRACT

The latest Mesoproterozoic Arctic Bay Formation (Borden Basin, Nunavut, Canada) is up to ~1130 m-thick and contains a significant proportion of unusually organic-rich black shale (up to 12.3 wt% total organic carbon). Insofar as increased biological productivity is related to organic matter burial, this organic-rich succession is seemingly incongruent with the low biological productivity world hypothesised for much of the Proterozoic. To better understand the conditions leading to development of this organic-rich unit, we explore the redox geochemistry of the Arctic Bay Formation using a multi-proxy approach (nitrogen isotopes, iron speciation, total organic carbon, total sulphur, and trace metal abundances). Redox proxy data support a stratified water column, with oxic surface waters underlain by intermittently euxinic waters, which are in turn underlain by persistently ferruginous deeper waters. The highly alkaline, restricted marine basin in which the Arctic Bay Formation was deposited may have allowed for rapid sequestration of highly reactive iron in carbonate minerals, resulting in an 'excess' of sulphur that resulted in sulphurisation of organic matter. Estimates for organic matter burial rates during deposition of the Arctic Bay Formation suggest that they were perhaps ~5–6 times mid-Proterozoic average values (although there are permissible scenarios in which it was extremely productive), underscoring that such organic-rich sedimentary rocks could be produced in a low productivity world.

© 2020 Published by Elsevier B.V.

## 1. Introduction

Much of the Proterozoic was likely marked by low oxygen abundance in the atmosphere and oceans, likely less than 10% of present atmospheric oxygen levels (PAL), and perhaps even less than 1% PAL (Cole et al., 2016; Canfield et al., 2018; Planavsky et al., 2018a, 2018b). Investigations of sustained low atmospheric  $pO_2$  levels during the mid-Proterozoic (ca. 2.0 to 0.8 Ga; Hodgskiss et al., 2019) have suggested an inextricable link between maintenance of a low oxygen world and low biological productivity (e.g., Derry, 2015). It has been suggested that low biological productivity would be a natural consequence of less efficient phosphorous

recycling between the water column and sediments under anoxic conditions, limiting the supply of bioavailable phosphorus (Derry, 2015; Laakso and Schrag, 2014, 2018; Ozaki et al., 2019; Reinhard et al., 2017). Recent studies combining empirical data and numerical modelling techniques also support a low productivity-low  $pO_2$  hypothesis.  $\Delta^{17}O$  anomalies recorded in sulphate minerals have been used to infer that gross primary production was ~6% of modern levels through much of the Proterozoic (Crockford et al., 2018, 2019; Hodgskiss et al., 2019), consistent with the range of 1 to 10% of modern net primary production suggested by Laakso and Schrag (2019), although the relationship between these two measures is not necessarily straightforward. While biological productivity is highly variable both regionally and seasonally (Vallina et al., 2014), and organic carbon burial rates differ significantly between the continental margin and deep sea (Burdige, 2007), the spatial distribution of productivity and organic carbon burial dur-

\* Corresponding author.

E-mail address: msw@stanford.edu (M.S.W. Hodgskiss).

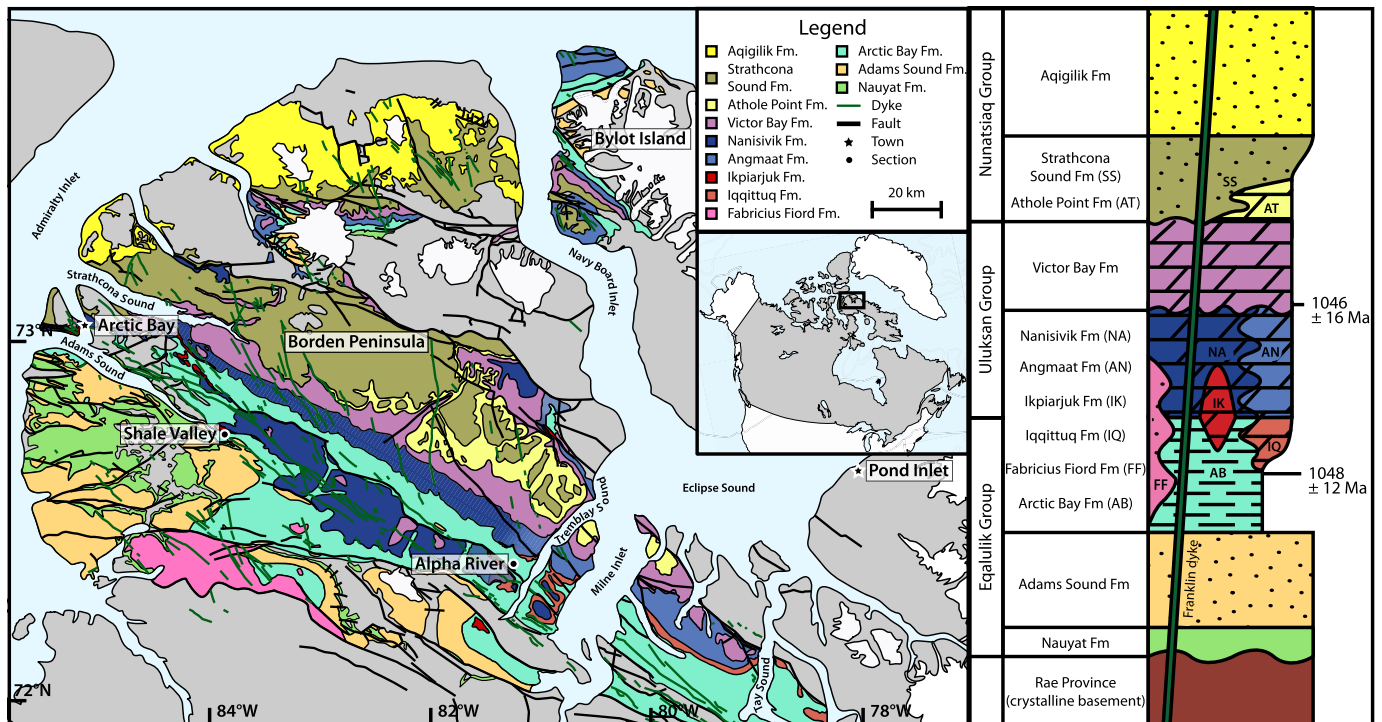


**Fig. 1.** Geological map and simplified stratigraphic column of the Bylot Supergroup on northernmost Baffin Island, Nunavut, Canada (modified from Hodgskiss et al., 2018). Colours in stratigraphic column (replotted from Turner, 2009) correspond to the stratigraphy in the geological map. Re-Os depositional ages from Gibson et al. (2018). (For interpretation of the colours in the figure(s), the reader is referred to the web version of this article.)

ing the Proterozoic remains an outstanding question (Olson et al., 2013; Reinhard et al., 2016; Laakso and Schrag, 2019).

The highly variable nature of organic matter deposition in the mid-Proterozoic lends credence to the idea that localised, anomalous regions of high productivity and/or enhanced preservation could have played an outsized role in global organic carbon burial. The latest Mesoproterozoic Arctic Bay Formation ( $1048 \pm 12$  Ma; Gibson et al., 2018) of the Bylot Supergroup, Nunavut, Canada (Fig. 1) may represent one such region, comprising a notably thick interval of organic-rich black shale (Figs. 2, 3; Hahn and Turner, 2017). Interpretations of Rock-Eval data, organic matter type and quality, and burial history suggest that the initial petroleum potential of the Arctic Bay Formation could have been five times greater (in millions of barrels/km<sup>2</sup>) than that of high-quality Phanerozoic source rocks in the Gulf of Mexico or West Africa (Fustic et al., 2017). The Arctic Bay Formation, although containing significantly more TOC (total organic carbon) than most mid-Proterozoic shale units (Fig. 3), is not the sole very high-TOC mid-Proterozoic shale; other units include the 1.38 Ga Velkerri Formation, Australia (~800 m-thick and up to 8 wt% TOC; Cox et al., 2016; Jarrett et al., 2019), the ca. 1.38 Ga Xiamaling Formation, China (~130 m-thick and up to 20 wt% TOC; Zhang et al., 2016; Diamond et al., 2018), and the 1.1 Ga Atar Group, Mauritania (tens of meters thick and up to 15 wt% TOC; Gilleaudeau and Kah, 2015). These organic-rich units are seemingly at odds with the diminished biological productivity expected during the mid-Proterozoic. However, it is conceivable these high TOC rocks are the result of either highly efficient export and burial of organic matter, low sedimentation rates (i.e., little dilution of organic matter by clastic material), or a combination of the two. Organic matter preservation potential (and thus, export and burial efficiency) is largely determined by the extent of organic matter remineralisation as a function of oxygen exposure time, which can be affected by recycling within the upper water column, settling through the water column, and overall burial rate in the sediment (Katsev and Crowe, 2015). These processes in turn

depend on factors such as the oxidising capacity of the water and sediment columns (i.e., abundance of O<sub>2</sub>, NO<sub>3</sub><sup>-</sup>, MnO<sub>2</sub>, SO<sub>4</sub><sup>2-</sup>, etc.), sedimentation rates, and clay mineralogy of the sediment (Canfield, 1994; Hedges and Keil, 1995; Kennedy et al., 2002; Tosca et al., 2010; Katsev and Crowe, 2015; Hemingway et al., 2019).

To better understand TOC preservation in ancient sedimentary units and the potential significance of this on the carbon cycle and Earth system as a whole, we explore this question in the Arctic Bay Formation by combining multiple independent geochemical proxies (iron speciation, trace element abundances,  $\delta^{15}\text{N}$ , TOC, and total sulphur) to characterise the prevailing redox conditions during deposition of the Arctic Bay Formation. We integrate these data with published age constraints and a Monte Carlo simulation comparing organic matter (OM) burial in the Arctic Bay Formation to calculated global averages for the Proterozoic Eon.

### 1.1. Geological context

The Bylot Supergroup is a sedimentary succession up to 6100 m-thick exposed on northernmost Baffin Island and Bylot Island, Nunavut, Canada (Fig. 1). At the base of the succession is the Nauyat Formation, which contains a basal quartzite sandstone unit overlain by a series of subaqueous tholeiitic basalt flows (Jackson and Ianelli, 1981). Above this, the Adams Sound Formation is composed of quartz arenite deposited in shallow marine environments (up to 610 m-thick; Long and Turner, 2012). This unit is overlain by the Arctic Bay Formation, which ranges in thickness from 180 to 1130 m, thinning toward the present-day northwest. The lower Arctic Bay Formation is composed of shallowing-upward cycles of shale, siltstone, and sandstone, overlain by organic-rich black shale, which is in turn overlain by interbedded black shale, silty shale, and siltstone without conspicuous cycles in the upper part of the unit. Deposition of the Arctic Bay Formation is inferred to have occurred during a time of relatively high subsidence rates caused by active normal faulting within the Borden Basin (Turner

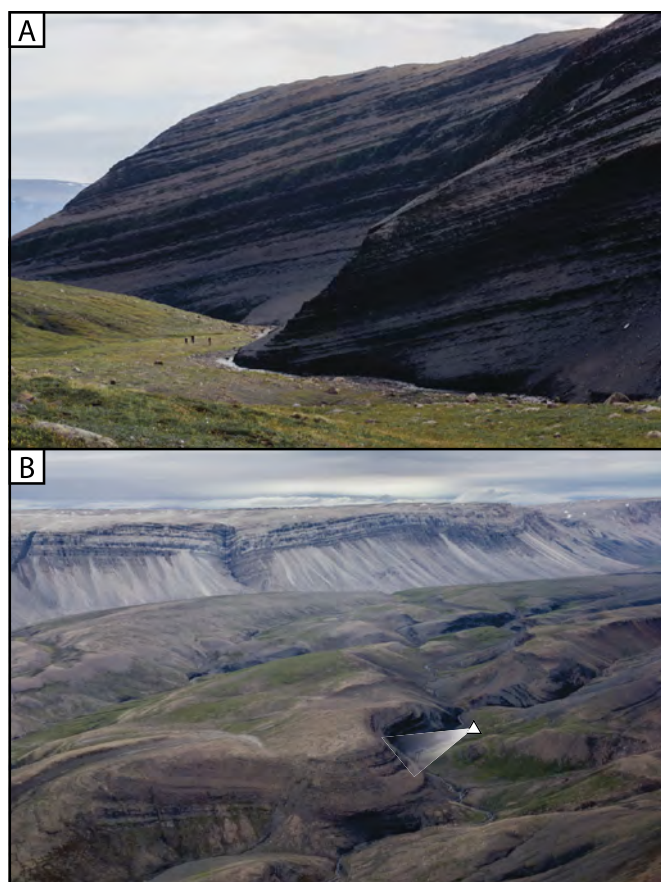


**Fig. 2.** Outcrops of the Arctic Bay Formation at Alpha River. A) A highly organic-rich interval of the Arctic Bay Formation in the variably euxinic to ferruginous zone. Note three people on grass at centre left for scale. B) View of Arctic Bay Formation exposed with the overlying Iqqittuq and Angmaat formations forming prominent grey cliffs in the distance. White triangle and gradient indicate location and approximate field of view for Fig. 2A.

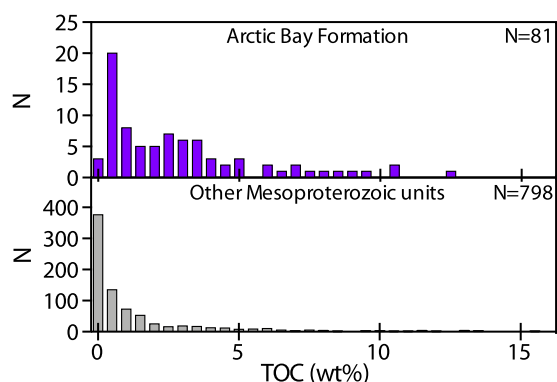


**Fig. 3.** Histogram of TOC contents from the Arctic Bay Formation compared to compiled Mesoproterozoic TOC contents from 30 different shale units, including the Velkerri and Xiamaling formations and the Atar Group. A Kolmogorov-Smirnov test returns a p-value of  $<0.0001$ , supporting that TOC contents in the Arctic Bay Formation are statistically different (i.e., higher) from most Mesoproterozoic shale units, although both datasets are likely subject to significant sampling biases.

and Kamber, 2012). Low angle erosional surfaces have been observed within the Arctic Bay Formation and are interpreted as the result of over-steepening due to syn-depositional faulting (Turner and Kamber, 2012). Similarly, breccia and conglomerate wedges localised along graben flank in the laterally equivalent Fabricius Fiord Formation record active faulting contemporaneous with deposi-

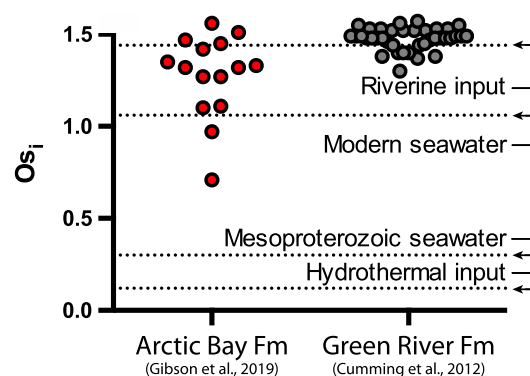


**Fig. 4.** Initial osmium isotope values ( $Os_i$ ) from the Arctic Bay Formation are consistent with a lacustrine depositional environment when compared with the Green River Formation (Cumming et al., 2012) and modern hydrothermal, seawater, and fluvial values (Peucker-Ehrenbrink and Ravizza, 2000), as well as inferred Mesoproterozoic seawater (Rooney et al., 2010). However, if osmium was not well-mixed in the oceans, these values may reflect a highly restricted (and perhaps intermittently lacustrine) basin rather than a stable lacustrine setting. Note that the sample with the lowest  $Os_i$  value in the Arctic Bay Formation is the stratigraphically highest sample, near the transition with the overlying Angmaat/Nanisivik Formations, which reflect marine environments (Gibson et al., 2019).

tion of the Arctic Bay Formation (Jackson and Ianelli, 1981). While herringbone crossbedding in the lower Fabricius Fiord Formation indicates deposition in a tidal environment, the remainder of this unit is composed of coarsening upward cycles superimposed on a larger-scale coarsening-upward trend, indicative of a prograding fan delta complex, with no further sedimentary evidence for tidal influence (Jackson and Ianelli, 1981). At this time, the basin gently deepened toward the present-day northwest (Turner and Kamber, 2012).

In the southeastern Borden Basin, the upper Arctic Bay Formation grades into the Iqqittuq Formation, which comprises approximately 380 m of interbedded dolomicrite and shale deposited on a northwest-prograding carbonate ramp. In the deeper, northwest portion of the basin and coeval with the upper Arctic Bay and Iqqittuq formations is the Ikpiarjuk Formation, which forms a series of isolated dolostone mounds located along major contemporaneous graben-bounding faults (Hahn et al., 2015). These carbonate mounds are interpreted as having formed via fluid venting along active normal faults into basin waters (Hahn and Turner, 2017). The Ikpiarjuk Formation interfingers with the Arctic Bay Formation, as well as the overlying Iqqittuq and Nanisivik formations. However, deposition of Ikpiarjuk mounds is thought to have ceased prior to deposition of the Nanisivik-Angmaat carbonate system and interstratification with these lower Ulukuan Group units owes to subaqueous to subaerial erosion of relict mound top relief and onlapping during subsequent shoaling (Hahn et al., 2015). The Arctic Bay and Ikpiarjuk formations in the northwest and Iqqittuq Formation in the southeast are all overlain by the carbonate-dominated Nanisivik and Angmaat formations. The ~520 m-thick Angmaat Formation was deposited as a rimmed carbonate platform with peritidal environments on the platform interior in the southeast. The Nanisivik Formation, which is composed of ~100 m of finely laminated dolostone with minor intraclast conglomerate in the northwest, represents the distal, basal facies correlative with the Angmaat Formation (Turner, 2009).

## 1.2. Hydrologic context of the Arctic Bay Formation

Based on rare earth element plus yttrium (REE + Y) trends of shale samples, Turner and Kamber (2012) suggested that the Arctic Bay Formation was deposited in a restricted basin. Hahn



et al. (2015), Hahn and Turner (2017) noted that REE + Y signatures of carbonate samples from the Ikpiarjuk Formation (contemporaneous with the upper Arctic Bay Formation) resemble modern alkaline lakes and inferred that deposition of the Arctic Bay Formation therefore took place in a similar environment. More recently, a lacustrine origin for the Arctic Bay Formation has been suggested by osmium isotope ratios, specifically highly 'evolved' initial osmium isotope values ( $Os_i$ ) ranging from 0.71 to 1.56 (Fig. 4; Gibson et al., 2019). These values overlap with those of the lacustrine Green River Formation ( $Os_i = 1.41$  to  $1.54$ ; Cumming et al., 2012) and modern riverine values ( $Os_i = 1.44$ ; Peucker-Ehrenbrink and Ravizza, 2000), and contrast with the 'primitive' signature from hydrothermal sources ( $Os_i = 0.12$ ; Peucker-Ehrenbrink and Ravizza, 2000) and inferred seawater values of  $\sim 0.30$  from the ca. 1100 Ma Atar Group in Mauritania (Rooney et al., 2010). While the radiogenic  $Os_i$  in the Arctic Bay Formation indicates a major influence from a local, evolved continental source (Gibson et al., 2019), it is worth noting that the residence time of Os in the Proterozoic is poorly constrained and may have approached the mixing time of the ocean (Rooney et al., 2016). Moreover, the residence time may have been further shortened under the more reducing conditions of the Proterozoic (Oxburgh, 2001), which could have resulted in Os isotope heterogeneity in the ocean, as suggested by Kendall et al. (2009a, 2009b). It should be noted, however, that the least radiogenic Os isotope value from the Arctic Bay Formation (0.71) occurs just before the transition to marine carbonate deposition throughout the basin. This value likely represents an increased proportion of Os from the marine reservoir, indicating that even if seawater was not homogeneous with respect to its Os isotope composition, the high values throughout the Arctic Bay Formation require limited marine influence. Conversely, high Mo (up to 50 ppm) and S (up to  $\sim 3$  wt%) concentrations in Arctic Bay Formation black shale suggest access to large reservoirs of these elements (Turner and Kamber, 2012), and therefore, some degree of sustained marine input.

Cumulatively, geochemical data indicate the Arctic Bay Formation was deposited in a restricted setting, though the precise degree and timescale of basin restriction remains unknown.  $Os_i$  isotope data suggest limited, if any, mixing with seawater, and REE + Y trends are similar to those from alkaline lakes. The high Mo and S contents in Arctic Bay Formation shales, however, suggest at least intermittent input from significantly larger Mo and S reservoirs than would generally be expected from a stable lacustrine setting. Although highly alkaline conditions have been suggested based on the carbonate mound geochemistry (Hahn et al., 2015), these mounds are of very limited geographic extent, calling into question their significance for increasing alkalinity at a basin scale. Major element and REE data of the Arctic Bay Formation are consistent with being sourced from basalt of the Nauyat Formation (Hahn et al., 2015). In this case, runoff from weathering of Nauyat Formation basalt, exposed along basin-margin horsts, may have helped to elevate alkalinity at a basin scale. However, Neodymium isotope ( $\epsilon Nd$ ) data throughout the Arctic Bay Formation, which range from  $-16.4$  to  $-11.3$ , are consistently more 'evolved' than Nauyat Formation basalt, which have a  $\epsilon Nd$  composition of  $-5.6$  (Gibson et al., 2019). Rather, this alkalinity may have instead been sourced from weathering of the Archean–Paleoproterozoic Rae craton crystalline basement surrounding the basin. Furthermore, unambiguously marine sedimentary structures, such as herringbone crossbedding, were not observed in the Arctic Bay Formation, and the ongoing tectonism throughout deposition of the Bylot Supergroup makes it difficult to confidently rely on marine sedimentary structures in strata under- or overlying the Arctic Bay Formation, given the possibility for tectonic readjustment of the basin (e.g., Sherman et al., 2002). The occurrence of herringbone crossbed-

ding within the laterally-equivalent lower Fabricius Fiord Formation, however, indicates a tidal (i.e., marine) influence elsewhere in the Borden Basin during deposition of the lower Arctic Bay Formation (Jackson and Ianelli, 1981). In summary, it seems most likely that deposition of the Arctic Bay Formation took place in a basin that was restricted (and perhaps intermittently isolated), but also at least intermittently received input of seawater, analogous to the modern Black Sea.

## 2. Materials and methods

### 2.1. Sample collection

Samples of the Arctic Bay Formation were collected from outcrops at two locations on the Borden Peninsula of northern Baffin Island, Nunavut. At Shale Valley (section T1413; N72.75133°, W83.84422°), samples were collected from a 358 m-thick stratigraphic section starting in the lower Arctic Bay Formation and stopping at the contact with the overlying Ikpiarjuk Formation. At Alpha River (sections PWC1405 and MB1401; N72.39550°, W81.18947°), two partial stratigraphic sections were combined to form a complete, 1130 m-thick composite section that begins at the contact with the underlying Adams Sound Formation and ends at the contact with the overlying Iqqittuq Formation.

### 2.2. Geochemical analyses

In total, 81 samples of the Arctic Bay Formation were studied using geochemical proxies. Weathered portions were cut off using a diamond saw, and the remaining sample was washed, dried, and crushed in a chrome-steel ring mill. Crushing soft rocks such as shale has been shown to result in negligible iron addition (Hickson and Juras, 1986; Sperling et al., 2013; Kunzmann et al., 2017).

Total carbon and sulphur analyses were conducted in triplicate by combustion of  $\sim 150$  mg of sample powder using an Eltra CS800 carbon/sulphur analyser at McGill University. To determine TOC content, raw sample powder was treated with 6 M HCl for 48 h to remove carbonate carbon. After rinsing and drying, the carbonate fraction was determined by gravimetry and the decarbonated powder was measured in the carbon/sulphur analyser. Analyses were calibrated using carbon and sulphur standards from Alpha Resources; measurement precision was better than 5%, and values were typically within 10 to 15% of published values.

Analyses of nitrogen and organic carbon isotope ratios were conducted at l'Institut Universitaire Européen de la Mer using aliquots of the previously decarbonated sample powders. Samples were weighed into tin capsules, such that each sample contained  $\sim 100$   $\mu g$  of organic carbon. Samples were combusted in a Thermo Scientific Flash 2000 elemental analyser coupled to a Thermo Scientific Delta V Plus isotope ratio mass spectrometer operating in continuous flow mode.  $\delta^{15}N$  and  $\delta^{13}C_{org}$  values are reported in permil, relative to atmospheric nitrogen and Vienna Pee Dee Belemnite, respectively. Isotopic measurements were calibrated against standard reference materials IAEA-N1, IAEA-N2, and in-house reference materials (LIPG – yeast from the Institut de Physique du Globe de Paris, acetanilide, caffeine, and leaf litter). Analytical uncertainties for  $\delta^{15}N$  and  $\delta^{13}C_{org}$  measurements were 0.3‰ and 0.2‰, respectively ( $\pm 1\sigma$ ).

Iron speciation was conducted at McGill University using the sequential extraction protocol developed by Poulton and Canfield (2005), where operationally-defined iron pools (iron carbonates, iron oxides, and magnetite) are selectively leached in a stepwise fashion using acetate, dithionite, and oxalate solutions, respectively. The leachates from each step were analysed for iron concentration using a PerkinElmer AAnalyst 100 atomic absorption spectrometer. Pyrite sulphur contents were extracted following the

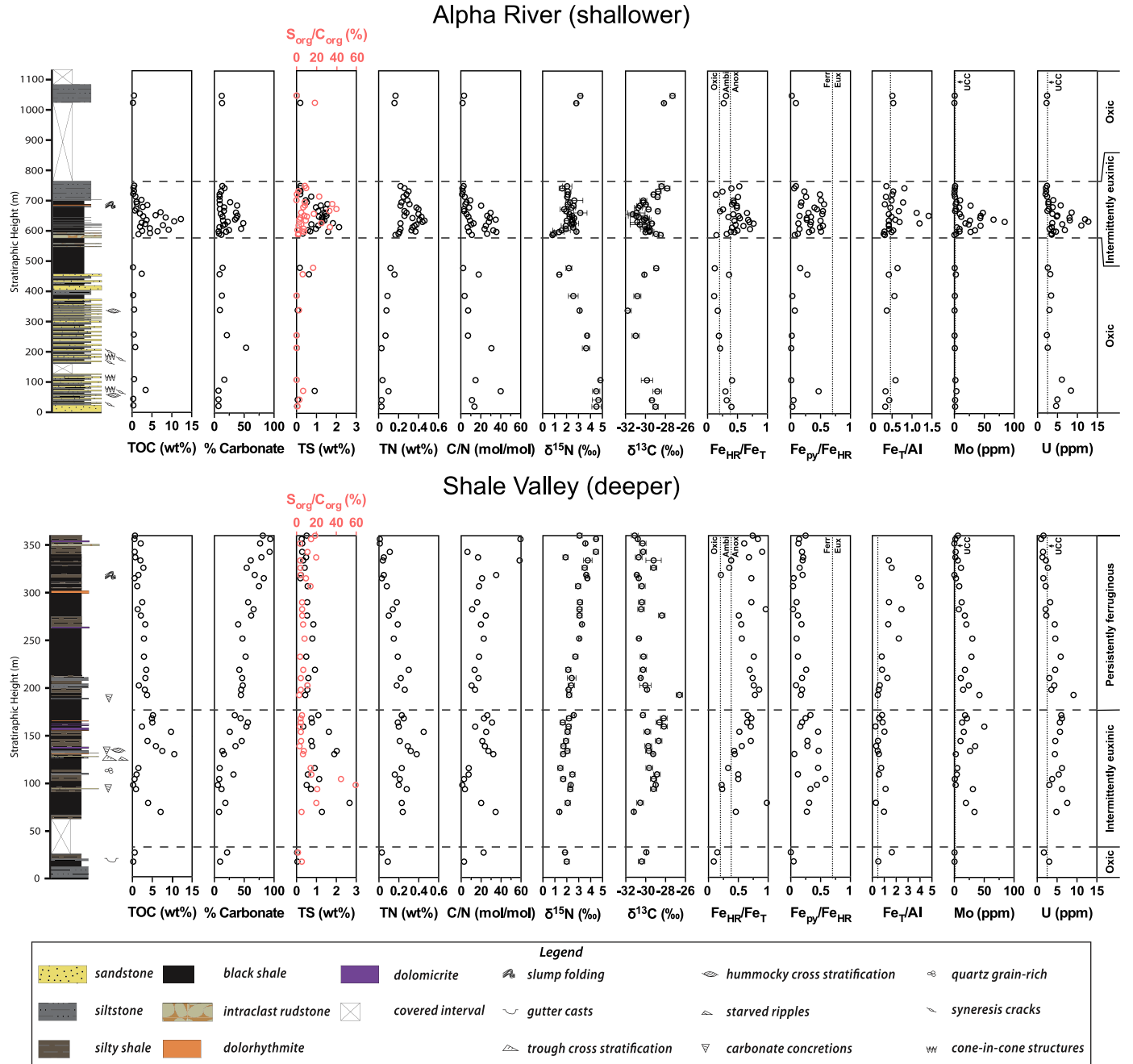


**Fig. 5.** Lithostratigraphy and chemostratigraphy for measured sections at Alpha River (relatively shallow) and Shale Valley (relatively deep), along with interpreted 'redox facies'. The stratigraphic section from Alpha River is interpreted to record a shift from oxic surface waters to an intermittently euxinic interval, then back to oxic surface waters, whereas the section from Shale Valley is interpreted to record a shift from oxic surface waters to intermittently euxinic waters, then persistently ferruginous basinal waters. Two samples near the top of the Shale Valley section with very low TN contents were excluded from the C/N plot. UCC = upper continental crust. Note that  $S_{org}$  is calculated, where  $S_{org} = S_{total} - S_{pyrite}$ . Refer to Sections 4.2 and 4.3 for detailed interpretation.

chromium reduction method of Canfield et al. (1986) and quantified by gravimetry. Iron in pyrite was calculated stoichiometrically from the pyrite sulphur contents. Repeat analyses of samples yielded a precision of 11%.

Trace element concentration analyses were conducted at Yale University. Samples were ashed at 500 °C for 8 h to remove organic matter. These samples were then digested at 90 °C using concentrated mixtures of HF-HNO<sub>3</sub> and HNO<sub>3</sub>-HCl. Samples were analysed using a Thermo Finnigan Element XR inductively coupled plasma mass spectrometer. Measurement precision was better than 4%, and analysis of standard reference materials (USGS BHVO-2 and NOD-A-1) were within 10% of published values.

### 3. Results

#### 3.1. Stratigraphic sections

A 1130 m-thick complete, composite section of the Arctic Bay Formation was measured at Alpha River (Fig. 5). Directly and conformably overlying the Adams Sound Formation, the lowest ~450 m of this section are composed of individually shallowing-upward shale-siltstone-sandstone cycles. Occasional occurrences of small-scale hummocky cross-stratification (HCS) in this interval indicate deposition above storm wave base. The following ~250 m consist of black shale (Fig. 2) with very minor beds of siltstone, dolomi-

crite, and lenses of intraclast rudstone (perhaps derived from shedding of a nearby Ikpiarjuk Formation carbonate mound). No HCS or current structures were observed in this interval. Most of the uppermost 450 m of the section are covered, but ~120 m of siltstone is exposed. The stratigraphic section ends at the base of carbonate beds of the overlying Iqittuq Formation.

At Shale Valley, a 358 m-thick partial section of the Arctic Bay Formation was measured (Fig. 5). The lowest ~25 m are composed of intercalated finely laminated siltstone intervals, thin sandstone beds with gutter casts, and silty, gray to black shale. Following ~50 m of cover, the formation is dominated by fissile black shale and silty, gray shale, with minor shale-siltstone-sandstone coarsening upward cycles and dolomitic concretions, dolomitic shale and siltstone and a meter-scale dolomicrite beds. Small-scale HCS, ripple-scale trough cross-stratification, and starved ripples occur in thin sandstone beds at ~130 m stratigraphic height. At the top of the section, an intraclast rudstone bed, slump folding, and convolute bedding occur just before the transition to pure carbonate facies of the overlying Ikpiarjuk Formation.

### 3.2. Total organic carbon, sulphur, and nitrogen contents

At Alpha River, TOC values are typically ~0.5 wt%, with the exception of the interval from 590 to 715 m, where TOC contents reach a maximum of 12.3 wt% (Fig. 5). Similarly, sulphur contents are typically ~0.05 wt%, reaching a maximum of 2.1 wt% in the middle interval. Nitrogen content steadily increases from ~0.05 wt% to a maximum of 0.5 wt% in the middle interval. Samples from Shale Valley show relatively low TOC values (<0.6 wt%) for two samples in the lowest 67 m, followed by generally high, although variable values (0.2 to 10.5 wt%) for the interval from 67.2 to 126.5 m (Fig. 5). TOC then steadily declines to a background level of ~2 to 3 wt%. Sulphur contents show a similar trend, rising from <0.05 wt% to ~1.5 wt%, followed by a steady decrease to approximately 0.5 wt%. Nitrogen contents follow a smooth arc rising from ~0.1 to 0.25 wt%, before steadily decreasing to <0.1 wt%.

### 3.3. Nitrogen and organic carbon isotopes

At Alpha River,  $\delta^{15}\text{N}$  values decrease from ~+4.8‰ to +0.8‰ from the base of the section to 590 m, before increasing to ~+2 to +3‰, where  $\delta^{15}\text{N}$  remains steady through the remainder of the section.  $\delta^{13}\text{C}_{\text{org}}$  values decline from -28‰ to -32‰ and return to -28‰ by 500 m (Fig. 5). A similar, albeit much more stratigraphically condensed trend, occurs from 590 to 750 m. In Shale Valley,  $\delta^{15}\text{N}$  values show a steady progression from +2‰ to +4‰ over the stratigraphic section (Fig. 5).  $\delta^{13}\text{C}_{\text{org}}$  values show variations of 1 to 2‰ that are centred around -30‰.

### 3.4. Iron speciation

To distinguish between oxic, ferruginous, and euxinic settings, iron speciation data are evaluated based on their division into operational pools. Evaluation of oxic versus ferruginous/euxinic (anoxic) environments is done using the ratio of highly reactive iron to total iron ( $\text{Fe}_{\text{HR}}/\text{Fe}_{\text{T}}$ ; the sum of iron in carbonates, oxides, magnetite, and pyrite divided by total iron;  $\text{Fe}_{\text{carb}}$ ,  $\text{Fe}_{\text{ox}}$ ,  $\text{Fe}_{\text{mag}}$ ,  $\text{Fe}_{\text{py}}$ , and  $\text{Fe}_{\text{T}}$ , respectively). Ratios of  $\text{Fe}_{\text{HR}}/\text{Fe}_{\text{T}}$  above 0.38 indicate anoxic conditions (Raiswell and Canfield, 1998; Raiswell et al., 2018), although samples deposited under anoxic water columns during rapid sedimentation can show muted enrichments. Samples with  $\text{Fe}_{\text{HR}}/\text{Fe}_{\text{T}} < 0.20$  likely represent oxic conditions (based on the lowest anoxic values in the modern ocean; Sperling et al., 2016), whereas values between 0.20 and 0.38 are ambiguous and may reflect deposition under oxic or anoxic conditions (Raiswell et al., 2018). To distinguish ferruginous from euxinic settings, the ratio

of iron in pyrite to all highly reactive iron ( $\text{Fe}_{\text{py}}/\text{Fe}_{\text{HR}}$ ) is considered, where  $\text{Fe}_{\text{py}}/\text{Fe}_{\text{HR}}$  values below 0.7 are indicative of deposition under ferruginous conditions, and values exceeding 0.7 indicate deposition under euxinic conditions (Raiswell et al., 2018).

At Alpha River, samples fall in the oxic or 'ambiguous' field, except for the interval from 590 to 715 m, where the vast majority record anoxic conditions.  $\text{Fe}_{\text{py}}/\text{Fe}_{\text{HR}}$  values show a similar trend, with near-zero values everywhere except the middle interval, where values reach up to 0.55 (Fig. 5). Total iron to aluminium ratios ( $\text{Fe}_{\text{T}}/\text{Al}$ ) generally range from 0.4 to 0.6, with several samples reaching up to 1.4 in the middle interval. In Shale Valley, the majority of samples fall within the anoxic field, and only a small portion within the ambiguous field. All  $\text{Fe}_{\text{py}}/\text{Fe}_{\text{HR}}$  ratios are below the euxinic threshold, although a distinct rise to a maximum of 0.58 near 100 m is observed (Fig. 5).  $\text{Fe}_{\text{T}}/\text{Al}$  ratios generally range from 0.3 to 1.0, increasing in the upper third of the section, where they reach up to 4.1.

### 3.5. Redox sensitive elements

At Alpha River, molybdenum (Mo) concentrations at the base of the section are generally low (~1 to 3 ppm), with a pronounced spike reaching 84 ppm near the middle of the section (Fig. 5). Uranium (U) concentrations are typically near 3 ppm at the base, except for a pronounced spike to 13 ppm in the middle of the section. Finally, nickel (Ni) concentrations have 'baseline' values of ~50 ppm, with a pronounced spike exceeding 200 ppm near the middle of the section. When normalised to TOC, Mo still exhibits a large increase, whereas U and Ni have no coherent variation.

At Shale Valley, Mo concentrations start below 0.5 ppm, increase to ~50 ppm near the middle of the section, and gradually decrease to less than 10 ppm by the top of the section (Fig. 5). Uranium concentrations show a rise from ~1 to 3 ppm to 6 ppm, before gradually declining to ~1 ppm. Several samples show elevated U contents, up to ~30 ppm (also near 150 m). Finally, Ni contents show a gradual decrease from ~80 ppm to ~20 ppm at the top of the section. Like data from Alpha River, Mo exhibits coherent variations when normalised to TOC, whereas U and Ni do not.

## 4. Discussion

### 4.1. Stratigraphic context

The shift observed at Alpha River from sandstone-siltstone-shale cycles with occasional HCS in the lower Arctic Bay Formation to structureless black shale near the middle of the stratigraphic section is consistent with overall deepening up-section, and a transition to deposition below storm wave base. The occurrence of siltstones at the top of the section indicates a return to a higher energy environment. Similar to Alpha River, the section measured at Shale Valley broadly indicates deepening up-section, with a shift toward generally finer grained lithologies and the disappearance of sedimentary structures.

The stratigraphic section measured at Alpha River contains prominent shale-siltstone-sandstone cycles at the base, which are not as well developed at Shale Valley. Additionally, this section contains siltstones at the top of the formation, after which it is overlain by the Iqittuq Formation (interpreted to record initiation of a carbonate ramp; Turner, 2009). In contrast, the stratigraphic section measured at Shale Valley is dominated by shales and silty shales continuing to the top of the formation, where it is overlain by deep-water carbonates of the Nanisivik Formation. Cumulatively, these observations suggest that deposition of the Arctic Bay Formation at Alpha River occurred in a shallower, more energetic environment than that of Shale Valley, consistent

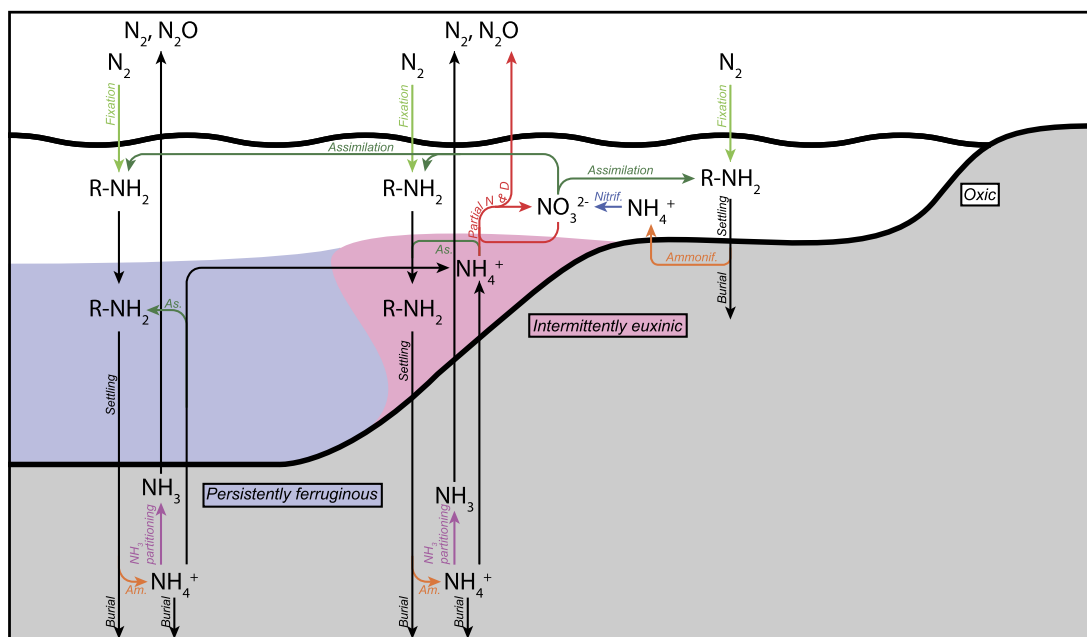


**Fig. 6.** Interpreted nitrogen cycle during deposition of the Arctic Bay Formation. While persistent or near-persistent oxic and ferruginous conditions dominate the shallowest and deepest portions of the basin, respectively, intermediate depths are variably euxinic to ferruginous. The shallowest waters are characterised by TOC/TN ratios near 4 and  $\delta^{15}\text{N}$  of  $\sim +3.5\text{‰}$ , whereas the deepest, ferruginous waters have a TOC/TN ratio of  $\sim 15$  and  $\delta^{15}\text{N} \sim +3.0\text{‰}$ . The intervening, variably euxinic to ferruginous waters reflect input from both water masses, with bimodal TOC/TN ratios of  $\sim 4$  and  $22$ .  $\delta^{15}\text{N}$  in this water mass are lighter,  $\sim +2\text{‰}$ , perhaps reflecting a comparatively high input of newly fixed nitrogen from the atmosphere (and consistent with a large OM flux). As. - Assimilation. Nitrif. - Nitrification. Am., Ammonif. - Ammonification. Partial N & D - Partial nitrification and denitrification.

with the interpretations of Turner (2009) and Turner and Kamber (2012). Further, the occurrence of siltstones near the top of the section at Alpha River suggests that the section shallowed-upward following deposition of the black shale packages in the middle interval, whereas Shale Valley continued with deposition in a deeper water environment and is overlain by the deepwater Nanisivik Formation. The observed sedimentary structures are ambiguous with respect to a marine or lacustrine setting because small-scale hummocky cross stratification and starved ripples can be produced in both settings (reviewed in Jones et al., 2020).

Direct correlation between the two measured stratigraphic sections could not be done, owing to the large distance ( $\sim 90$  km) between sections and the lack of marker beds. Additionally, Turner and Kamber (2012) identified large scale, low angle erosional surfaces within the Arctic Bay Formation, further complicating any possible correlation.

## 4.2. Redox stratification

Integrating our geochemical data into the stratigraphic framework presented here supports a redox-stratified water column with three distinct zones: oxic surface waters, an intermediate-depth region that likely experienced intermittently euxinic conditions, and ferruginous basinal waters (Figs. 5, 6). When  $\text{Fe}_\text{T}/\text{Al}$  ratios are compared against the standard value for oxic sediments (0.55; Raiswell et al., 2018), almost all Arctic Bay Formation measurements are depleted with respect to iron. However, these values were measured in open marine sediments and may not be directly applicable to the restricted marine environment discussed here. Alternatively, Gibson et al. (2020) showed that  $\text{Fe}_\text{T}/\text{Al}$  ratios can locally strongly differ from average crustal values, especially within restricted basins, and suggest establishing a local baseline. We take the mean value ( $0.46 \pm 0.11$ ) of the low TOC, oxic shales in the Arctic Bay Formation as a comparative baseline for oxic conditions.

### 4.2.1. Oxic surface waters

The shales of the oxic surface waters are characterised by  $\text{Fe}_\text{HR}/\text{Fe}_\text{T}$  values that are oxic to 'ambiguous', with  $\text{Fe}_\text{py}/\text{Fe}_\text{HR}$  values  $\sim 0$ , low TOC (generally  $\sim 0.5$  wt%), and  $\delta^{15}\text{N}$  values ranging from 2 to 5‰. Carbonate contents range from 7 to 53 wt%, with a mean of 16 wt%. Based on our local baseline,  $\text{Fe}_\text{T}/\text{Al}$  ratios show no authigenic iron enrichment. Redox sensitive elements such as Mo, U, and V are present at near-crustal values (mean of 1.3, 4.4, and 94 ppm respectively; Wedepohl, 1995).

### 4.2.2. Intermittently euxinic region

Underlying the oxic surface waters is a zone characterised by highly variable TOC values, ranging from 0.2 to 12.3 wt%.  $\delta^{15}\text{N}$  values are less positive than the oxic zone, typically  $+2\text{‰}$  with a range from  $+0.8$  to  $+2.5\text{‰}$ . Ratios of  $\text{Fe}_\text{HR}/\text{Fe}_\text{T}$  are  $\sim 0.5$  and  $\text{Fe}_\text{py}/\text{Fe}_\text{HR}$  values are as high as  $\sim 0.6$ . Iron contents are variable, with  $\text{Fe}_\text{T}/\text{Al}$  ranging from 0.27 to 1.42 (mean of 0.59). In the canonical iron speciation framework, these  $\text{Fe}_\text{HR}/\text{Fe}_\text{T}$  and  $\text{Fe}_\text{py}/\text{Fe}_\text{HR}$  values would be interpreted as representing deposition under ferruginous waters. However, significant enrichment of redox sensitive elements such as Mo, U, and V occur in this part of the Arctic Bay Formation, reaching up to 84, 24, and 877 ppm, respectively. Such enrichments likely indicate deposition in an intermittently euxinic environment (Lyons et al., 2009; Scott and Lyons, 2012). It has been suggested that pyritisation of iron oxides by sulphide can be kinetically inhibited in alkaline environments, based on modern observations, leading to the presence of reactive iron even in environments with high sulphide concentrations (Tuttle et al., 1990; see also discussion in Stüeken et al., 2019). Stüeken et al. (2019; and references therein) noted that iron solubility decreases with increasing pH, and suggested that in some alkaline environments, reduced iron may have been efficiently sequestered in carbonates rather than returning to the water column, potentially hindering pyrite formation. This is consistent with the iron speciation data from the Arctic Bay Formation, where  $\text{Fe}_\text{carb}$  often composes more than half of the highly reactive iron pool. One possibility is that



highly alkaline conditions during deposition of the Arctic Bay Formation may have been maintained by seepage of alkaline fluids along major faults and runoff from weathering of the surrounding Rae craton. The positive relationships between  $\text{Fe}_T/\text{Al}$  and  $\text{Fe}_{\text{carb}}$  ( $R^2 = 0.57$ ),  $\text{Fe}_{\text{HR}}/\text{Fe}_T$  and carbonate wt% ( $R^2 = 0.41$ ), and increasing carbonate content from oxic to intermittently euxinic to persistently ferruginous conditions, further highlight the significance of carbonate formation beneath strongly reducing waters. Finally, the amount of sulphur in non-pyrite phases in this redox facies of the Arctic Bay Formation is comparable to sulphur in pyrite (i.e., non-pyrite sulphur is often  $\sim 60\%$  of total sulphur), further implying an 'excess' of sulphur that did not react with highly reactive iron. This is similar to results from the (lacustrine) Paleocene Green River Formation, where alkaline conditions in a euxinic water column apparently resulted in sulphurisation of organic matter rather than complete pyritisation of highly reactive iron (Tuttle and Goldhaber, 1993). We therefore interpret these sedimentary rocks as having been deposited beneath a part of the water column with fluctuating redox conditions that were at least intermittently euxinic.

The fluctuating redox conditions postulated for this stratigraphic interval have been previously suggested for the mid-Proterozoic based on numerical modelling and geochemical data. Modelling by Reinhard et al. (2016) suggested that oceans in a low  $\text{O}_2$  world would be subject to significant variability in redox conditions both spatially and seasonally, owing to factors such as  $\text{O}_2$  production, the export of carbon, surface winds, and  $\text{Fe}^{2+}$  availability. Shale geochemical data from the 1.85 Ga Stambaugh Formation was interpreted by Planavsky et al. (2018a, 2018b) to reflect regional and temporal variability in redox conditions, perhaps as a result of deposition beneath a water column with only a small redox buffer.

#### 4.2.3. Ferruginous, basinal waters

The deepest, basinal waters are characterised by  $\text{Fe}_{\text{HR}}/\text{Fe}_T$  values of  $\sim 0.7$ , reaching up to 1.0.  $\text{Fe}_{\text{py}}/\text{Fe}_{\text{HR}}$  values are  $\sim 0.1$ , substantially lower than that of the intermittently euxinic region.  $\text{Fe}_T/\text{Al}$  reaches up to 4, although we note that the highest  $\text{Fe}_T/\text{Al}$  values correspond to the most carbonate-rich samples. This may be the result of efficient iron sequestration in carbonate phases under alkaline conditions (Stüeken et al., 2019), and is supported by the high carbonate abundance in these samples (ranging from 40 to 94 wt%, mean of 63 wt%). This interpretation is further supported by  $\text{Fe}_{\text{carb}}$  composing a significant pool of highly reactive iron ( $\text{Fe}_{\text{carb}}/\text{Fe}_{\text{HR}}$  ranges from 0.52 to 0.91, mean = 0.71). TOC values range from 0.5 to 3.7 wt%, and  $\delta^{15}\text{N}$  values range from +3 to +4.5‰. Redox sensitive elements are moderately enriched, above that of the oxic region but below the intermittently euxinic region, with Mo, U, and V means of 13, 5, and 191 ppm, respectively. Cumulatively, these sediments are interpreted to have been deposited under persistently ferruginous conditions where alkaline waters resulted in the efficient sequestration of iron in carbonate minerals.

#### 4.3. Nitrogen cycling in the Arctic Bay Formation

Before interpreting the Nitrogen isotope record of Arctic Bay Formation shale in the context of primary, depositional redox cycling, it is important to consider how isotopic values may have been affected by post-depositional processes. There is no relationship between total nitrogen (TN) and  $\delta^{15}\text{N}$ , or TOC and  $\delta^{15}\text{N}$  in our sample set, suggesting that preferential loss of isotopically light nitrogen did not occur. Further, TOC/TN ratios (mol/mol; Fig. 5) are generally consistent with those of other Precambrian sedimentary successions interpreted as recording  $\delta^{15}\text{N}$  values reflective of primary processes (e.g., Kipp et al., 2018). Finally, by standards for Mesoproterozoic strata, the Arctic Bay Formation has experienced

relatively low thermal maturation and is still in the dry gas window (calculated Ro% of  $\sim 1.4$ ; Fustic et al., 2017). The measured  $\delta^{15}\text{N}$  values are therefore considered to reflect primary processes, including processes in the water column and diagenesis in the uppermost sediment column.

Nitrogen isotope values within the Arctic Bay Formation fall between  $\sim +0.8$  and  $+4.8\text{‰}$ , similar to many Proterozoic successions (e.g., Ader et al., 2016). Paired with other redox proxies (e.g., iron speciation, trace element concentrations) and carbon to nitrogen ratios (TOC/TN), these data provide insight into ancient nitrogen cycling in this environment. Various processes in the nitrogen cycle (e.g., ammonia volatilisation, partial nitrification and denitrification) offer predictions for shifts in both  $\delta^{15}\text{N}$  and TOC/TN ratios, helping to eliminate nonunique solutions despite much of the  $\delta^{15}\text{N}$  data falling in a range of just several permil.

Given that iron speciation data demonstrate that the uppermost portion of the water column was oxic, underlain by anoxic deeper waters, the predominant nitrogen compounds in these parts of the water column were likely nitrate ( $\text{NO}_3^-$ ) and ammonium ( $\text{NH}_4^+$ ), respectively. Nitrogen fixation from the atmosphere ( $\delta^{15}\text{N} = 0\text{‰}$  by definition) by diazotrophs in surface waters would occur with only minor fractionation (Stüeken, 2013). In sediments deposited under anoxic, alkaline conditions, diagenetically released ammonium is partially converted to ammonia ( $\text{NH}_3$ ), leaving the residual ammonium  $^{15}\text{N}$ -rich (Stüeken et al., 2019). This ammonium can then be reassimilated by organisms or incorporated into clays in place of potassium (Müller, 1977; Stüeken et al., 2019). In addition to leaving the residual ammonium  $^{15}\text{N}$ -enriched, the preferential loss of nitrogen relative to carbon during this process results in elevated TOC/TN ratios (Stüeken et al., 2019). Fractionation from this process, in addition to the input of fixed nitrogen ( $\delta^{15}\text{N} = 0\text{‰}$ ), may explain the moderately enriched  $\delta^{15}\text{N}$  values ( $\sim +1.9$  to  $+4.5\text{‰}$ ) and TOC/TN ratios ( $\sim 7$  to 61, mean of 22) observed in the persistently ferruginous region (Fig. 5). The maximum  $\delta^{15}\text{N}$  values reported here are considerably less positive than those reported for other alkaline environments, possibly as a result of mixing with less alkaline seawater, lowering the pH to near or below the 9.2 threshold required for  $\text{NH}_3$  volatilisation (Stüeken et al., 2019, 2020).

Ammonium that mixed from either the ferruginous or intermittently euxinic regions into the overlying oxic water column (where  $\text{NO}_3^-$  is the dominant nitrogen compound) would have undergone partial nitrification and denitrification, with  $^{15}\text{N}$ -poor  $\text{N}_2$  and  $\text{N}_2\text{O}$  escaping to the atmosphere, leaving the residual nitrate in the water column  $^{15}\text{N}$ -enriched (Fig. 6). Within samples inferred to reflect deposition in the oxic surface waters,  $\delta^{15}\text{N}$  ranges from +1.9 to +4.8‰, which is almost identical to those from the deep, ferruginous waters. However, in addition to being characterised by oxic conditions (inferred from iron speciation data) and low TOC, these sediments have lower TOC/TN ratios ( $\sim 2$  to 40, mean of 13) than those of the ferruginous sediments (Fig. 5). These relationships suggest that the partitioning of ammonium to ammonia (and associated increase in TOC/TN ratios) was not a dominant process in sediments deposited beneath this portion of the water column, consistent with deposition under comparatively oxic conditions. Rather, the range of  $\delta^{15}\text{N}$  values in the oxic surface waters are interpreted as reflecting a balance between input of nitrogen fixed from the atmosphere and nitrogen that has undergone partial nitrification and denitrification.

In samples deposited during intermittently euxinic conditions,  $\delta^{15}\text{N}$  falls between +0.8 to +3.2‰, and there is considerable scatter in all geochemical proxies within this zone. For example, TOC ranges from  $\sim 0.2$  to 12.3 wt%, and Mo concentrations range from  $\sim 0.2$  to 84 ppm. TOC/TN ratios also vary considerably, and exhibit strong bimodality, with peaks at 5 and 22 (Figs. 5, 7). The considerable scatter in redox proxies in this region may be ex-



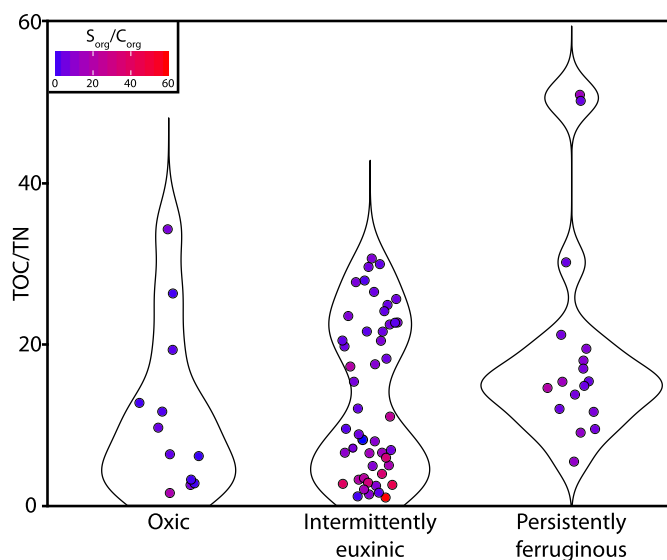


**Fig. 7.** 'Violin plot' of TOC/TN values for each of the redox facies. Data points are coloured according to  $S_{org}/C_{org}$  values (mol/mol%; where  $S_{org} = S_{total} - S_{pyrite}$ ). The highest  $S_{org}/C_{org}$  values occur in samples with low TOC/TN values in the intermittently euxinic region and are interpreted to represent the most intense sulphurisation of organic matter, potentially due to the fluctuating conditions in this redox facies.

plained in light of the bimodal TOC/TN ratios. Elevated TOC/TN ratios ( $\sim 15$  to  $25$ ) are interpreted to reflect sediments deposited in a strongly reducing environment associated with incomplete partitioning of ammonium to ammonia (Stüeken et al., 2019), whereas samples with lower TOC/TN ratios ( $\sim 1$  to  $10$ ) were deposited under less reducing conditions where nitrogen occurred as nitrate rather than ammonium, precluding this process. This interpretation is supported by other redox proxies (e.g., Mo, U, V,  $Fe_{HR}/Fe_T$ ), where values indicative of a more reducing environment co-occur on a relatively fine stratigraphic scale (at least with respect to our m-scale sampling) with elevated TOC/TN ratios. The lowest  $\delta^{15}N$  values in this interval, approaching  $0\text{‰}$ , are similar to that expected for an environment dominated by nitrogen fixation, and may reflect deposition during an interval of particularly efficient organic carbon burial with minimal early diagenetic or water column processes altering  $\delta^{15}N$ . Sediments in the intermittently euxinic redox facies are therefore interpreted as having been deposited under highly variable redox geochemistry, as indicated by the bimodality of TOC/TN ratios. Samples with lower TOC/TN ratios likely reflect deposition beneath an alkaline, comparatively oxic water column where the nitrogen cycle was dominated by partial nitrification and denitrification. Conversely, intervals with high TOC/TN ratios reflect deposition under an alkaline, strongly reducing water column with incomplete partitioning of ammonium to ammonia (Fig. 7). The small interval of near-zero  $\delta^{15}N$  values may represent an interval that was dominated by nitrogen fixation.

#### 4.4. Enhanced organic matter preservation via sulphurisation

There is generally a significant 'excess' of sulphur in shales from the Arctic Bay Formation with respect to the measured sulphur from pyrite. Specifically, non-pyrite sulphur comprises approximately 60% of total sulphur. These samples are generally unusually organic-rich, making it likely that the phase containing this 'excess' sulphur is organic matter. In order for sulphurisation (the formation of organic sulphur compounds) to occur, several requirements must be met: (i) there must be sufficient reactive organic matter, (ii) there must be limited quantities of reactive iron, and (iii) sufficient quantities of reduced sulphur species must be available

(Werne et al., 2004). Arctic Bay Formation shales are both rich in organic matter (up to 12.3 wt% TOC after degradation of organic matter via remineralisation and maturation), and appear to contain ample reduced sulphur species, given that samples average 0.7 wt% pyrite, with some reaching up to 2.7 wt%. Reactive iron may have been limited by its efficient sequestration in carbonate minerals, and the kinetic inhibition of pyrite formation under alkaline conditions would have increased  $H_2S$  concentrations (Tuttle et al., 1990).

The replacement of functional groups in organic matter by sulphur species reduces reactivity, making it more resistant to microbial recycling and degradation, thereby increasing preservation potential (Werne et al., 2004; Hülse et al., 2019). It has been suggested that oscillating redox conditions may also lead to enhanced sulphurisation, where degradation of OM produces reactive compounds for subsequent sulphurisation (Emmings et al., 2019). The intermittently euxinic region overall shows much higher  $S_{org}/C_{org}$  ratios (mol/mol%, where  $S_{org} = S_{total} - S_{pyrite}$ ) than either the oxic or persistently ferruginous regions (mean of 12 compared to 3 and 8, respectively), again supporting the hypothesis that redox fluctuations may enhance organic matter sulphurisation (Fig. 7). These  $S_{org}/C_{org}$  ratios are calculated from measurements of total sulphur and pyrite sulphur contents, rather than sulphur in organic matter, and could therefore have been affected by oxidative weathering of pyrite. However, we note that even if all iron oxides were derived from oxidation of pyrite during weathering,  $\sim 40\%$  of samples in the intermittently euxinic region still have an 'excess' of sulphur that could not be attributed to pyrite (or oxidative weathering of pyrite). Sulphurisation of organic matter in the Arctic Bay Formation may therefore help explain the high TOC values, although we note that anoxic conditions at depth (relative to surface waters) alone would have helped increase preservation of organic carbon (e.g., Canfield, 1994); the correlation between TOC and TOC/TN ( $R^2 = 0.54$  when removing two outliers with very low TN) is consistent with nitrogen loss under conditions that favour preservation of OM. However, anoxia alone seems unlikely to explain the significantly elevated TOC contents in the intermittently euxinic environment relative to the persistently ferruginous environment, given that they both record dominantly anoxic conditions.

#### 4.5. Significance of the Arctic Bay Formation in a low productivity world

Recent geochemical and modelling results have suggested that much of the mid-Proterozoic (ca. 2.0 to 0.8 Ga) was likely characterised by sustained low levels of primary production (Laakso and Schrag, 2019; Crockford et al., 2018, 2019; Ozaki et al., 2019; Hodgskiss et al., 2019). If net primary production was between 1 to 10% of modern levels (Laakso and Schrag, 2019) during deposition of the Arctic Bay Formation, how did these high TOC shales form in a low productivity world?

We calculate the organic carbon content of the Arctic Bay Formation using the modern day surface area of preserved strata from the Borden Basin ( $\sim 51800 \text{ km}^2$ ; approximately 90% the size of Lake Huron), a thickness of 220 m for the most organic-rich interval of the Arctic Bay Formation, a range of shale densities ( $2,400$  to  $2,700 \text{ kg/m}^3$ ), and a calculated average  $TOC_{initial}$  of 10.5 wt% based on Rock-Eval data (Fustic et al., 2017). Black shales within the organic matter-rich interval of the Arctic Bay Formation have been dated using Re-Os geochronology as  $1048 \pm 12 \text{ Ma}$ , and black shales at the base of the Victor Bay Formation, approximately 750 m stratigraphically higher, have been dated as  $1046 \pm 16 \text{ Ma}$  (Fig. 8A; Gibson et al., 2018). In order to evaluate an end-member scenario, if deposition of the stratigraphically higher, Nanisivik/Angmaat formations carbonate system took place effectively instantaneously relative to the Arctic Bay Formation, its

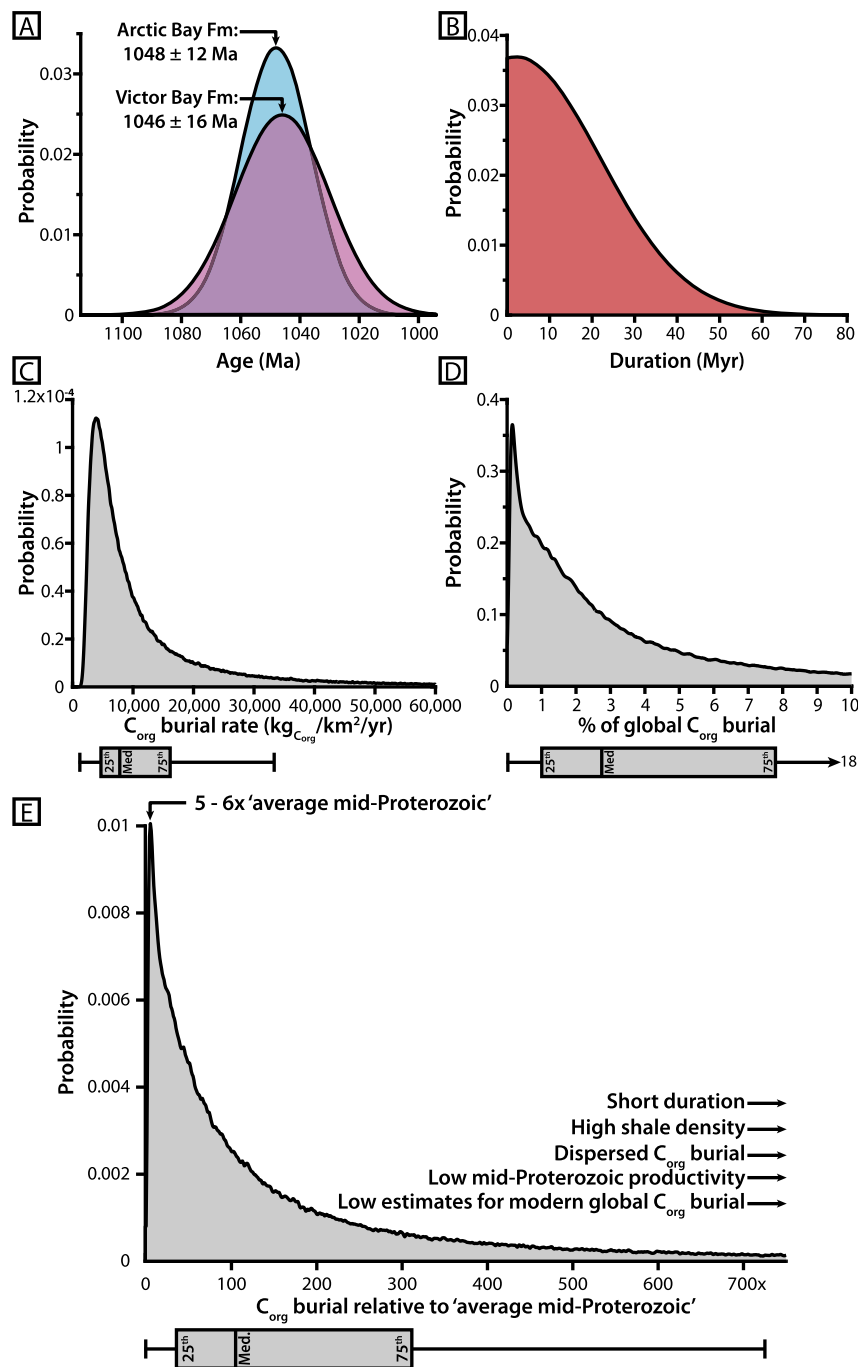


**Fig. 8.** Monte Carlo inputs and results. **A)** Re-Os age constraints for the Arctic Bay and Victor Bay formations from Gibson et al. (2018). **B)** Resampling depositional ages from Fig. 8A provides a wide range of depositional durations for the Arctic Bay Formation, assuming deposition of the overlying carbonate formations was effectively instantaneous. Note that non-physical scenarios (with the Arctic Bay Formation being younger than the Victor Bay Formation) were excluded. **C)** Monte Carlo results indicate that  $\sim 4,000$  kg of organic carbon were buried per  $\text{km}^2$  per year in the Arctic Bay Formation. **D)** The Arctic Bay Formation seems unlikely to have composed a significant component of global organic carbon burial, with a modal value of  $\sim 0.1\%$ , although the median value is  $\sim 3\%$ . **E)** Organic carbon burial rates in the Arctic Bay Formation need not have been remarkably high, with a modal value just 5–6 times higher than a calculated ‘average mid-Proterozoic’ rate. However, we note that there is an extremely long positive tail, and the median value is  $\sim 100$  times the ‘average mid-Proterozoic’ organic carbon burial rate.

deposition could have taken over  $\sim 0$  to 30 Myr, when considering  $2\sigma$  uncertainties on the depositional ages.

To explore the possible range of solutions for organic matter burial rates, we vary the shale density and resample Re-Os depositional ages from Gibson et al. (2018), including analytical uncertainties (but excluding resampling scenarios where the Arctic Bay Formation is younger than the overlying Angmaat and Victor Bay formations; Fig. 8B). Using a simple Monte Carlo simulation, these inputs suggest that the Arctic Bay Formation contains 2.9 to 3.2

$\times 10^{15}$  kg of organic carbon, with a modal accumulation rate of  $\sim 4,000$  kg of organic carbon per square kilometre per year (median of  $\sim 8,000$   $\text{kg}/\text{km}^2/\text{yr}$ ; Fig. 8C). This is higher than modern open marine basins, but consistent with modern intracontinental and terrestrial basins and calculated rates for Proterozoic lacustrine basins (Spinks et al., 2014). It should also be noted that this is a conservative estimate, considering this calculation uses the modern aerial extent of strata preserved above sea level from the Borden Basin, as well as the unrealistic end-member scenario

**Table 1**

Input parameters for Monte Carlo simulation to calculate organic carbon burial rates for the Arctic Bay Formation and the 'mid-Proterozoic average'.

Parameter	Value
Surface area of Arctic Bay Formation	51,800 km <sup>2</sup>
Shale density	2,400 to 2,700 kg/m <sup>3</sup>
TOC <sub>initial</sub>	10.5 wt%
Depositional duration	Between 1048 ± 12 Ma and 1046 ± 16 Ma
Estimates for global ocean organic carbon burial rates (modern)	$1.2 \times 10^{11}$ to $2.6 \times 10^{12}$ kg/yr
Net Primary Production (Proterozoic)	1 to 10% of modern levels
Modern ocean surface area	$3.6 \times 10^8$ km <sup>2</sup>
Portion of surface area beneath which organic carbon is buried	20 to 100%

in which Nanisivik/Angmaat carbonates were deposited instantaneously.

To compare the Arctic Bay Formation to 'average' mid-Proterozoic primary production, we integrate eleven different estimates of organic carbon burial rates in the modern ocean (ranging from  $1.2 \times 10^{11}$  to  $2.6 \times 10^{12}$  kg/yr; summarised in Burdige, 2007). These burial rates are scaled by 1 to 10% to accommodate for the smaller Proterozoic biosphere (Laakso and Schrag, 2019), although we note that relationships between net primary productivity, gross primary productivity, export production, and organic carbon burial are not straightforward, especially when considering the feedbacks at low O<sub>2</sub> levels (e.g., anoxia promotes OM burial, but enhanced OM burial in turn results in O<sub>2</sub> production). We also consider that most organic carbon burial occurs on continental margins (Hartnett et al., 1998), which only comprise ~20% of the modern ocean surface area (Walsh, 1991). An additional input is therefore integrated with the Monte Carlo simulation, normalising 'mid-Proterozoic production' between 20 to 100% of the surface area of the modern ocean (all parameters summarised in Table 1). Cumulatively, this allows calculated organic carbon burial rates in the Arctic Bay Formation to be compared against a hypothetical 'average rate' for mid-Proterozoic organic carbon burial. These results suggest that the Arctic Bay Formation may have accounted for ~0.1% of global organic carbon burial during its deposition, although there is a very long tail toward higher values, and the median is approximately 3% of global organic carbon burial (Fig. 8D). In other words, it would take ~1,000 coeval 'Arctic Bay Formation equivalents' to comprise all of mid-Proterozoic organic carbon burial when using the modal value, versus ~33 'Arctic Bay Formation equivalents' when using the median value. When the range of possible Arctic Bay Formation organic carbon burial rates and 'average mid-Proterozoic' organic carbon burial rates (both as kg<sub>CO<sub>2</sub></sub>/km<sup>2</sup>/yr) from the Monte Carlo model are compared, the Arctic Bay Formation is ~5 to 6 times higher than average 'mid-Proterozoic' values, although we again note a long positive 'tail' that can be attributed to model scenarios with short depositional durations, high shale density (and thus a larger mass of organic carbon), organic carbon burial occurring over a large area of the ocean rather than being concentrated on continental margins, and low estimates of modern organic carbon burial (Fig. 8E). Overall, these analyses demonstrate that the high TOC levels characterising the Arctic Bay Formation could be achieved with only moderate increases above hypothesised low global mid-Proterozoic organic carbon burial rates – it is an outlier but not unexplainable. Additionally, the widespread occurrence of anoxic conditions throughout the Mesoproterozoic suggests rem-

ineralisation of OM in the water and sediment columns was lower than in the modern ocean, meaning that net organic carbon burial rates may not have been proportionately suppressed, in spite of the significantly lower gross primary productivity suggested by Crockford et al. (2018, 2019). Furthermore, the restricted nature of the Borden Basin during deposition of the Arctic Bay Formation, which may have been a common feature of many coeval intracratonic basins, would have hindered circulation of basin waters, and further stabilised redox stratification. It is worth noting that estimates for global organic carbon burial in the modern Earth vary by more than an order of magnitude (Burdige, 2007), underscoring that the Arctic Bay Formation need not represent a mid-Proterozoic black shale succession with remarkably high organic carbon burial rates. Nonetheless, a scenario in which the Arctic Bay Formation records significantly elevated local primary productivity cannot be ruled out, with productivity possibly sustained by phosphorous derived from weathering of uplifted crystalline Rae craton (Horton, 2015). Considering episodically restricted epeiric seaways were relatively widespread at this time (Kah et al., 2012; Gilleaudeau and Kah, 2013, 2015), these environments may have been highly productive 'oases,' stimulated by elevated P delivered via continental weathering.

Laakso and Schrag (2019) noted that inefficient recycling of phosphorous in the Proterozoic would have resulted in the concentration of biological productivity around river mouths and estuaries, suggesting organic matter production (and burial) would have been more spatially concentrated than on the modern Earth. If organic carbon burial was concentrated in particular depositional loci during the Proterozoic, this would likely reduce the difference between the Arctic Bay Formation and 'average mid-Proterozoic' shale. Further, locally high primary productivity may have shifted the local water column toward more reducing conditions, as suggested for the intermittently euxinic region identified in the Arctic Bay Formation, potentially increasing local preservation potential (as suggested for some modern sites; e.g., Zimmerman and Canuel, 2000). The Monte Carlo simulation used here may be further complicated by a potential shift in the Earth system near the time of Arctic Bay Formation deposition. Crockford et al. (2019) interpreted  $\Delta^{17}\text{O}$  data from sulphate minerals in the overlying Angmaat Formation to represent a shift to higher levels of gross primary productivity than the preceding ~1 Gyr. If this shift to increased gross primary production occurred prior to deposition of the Arctic Bay Formation, organic carbon burial rates may have been higher, potentially reducing the observed difference between the Arctic Bay Formation and the 'average mid-Proterozoic'. Overall, these results highlight that across all levels of primary productivity, organic carbon deposition in the context of the carbon cycle is a diffuse, global process rather than being dominated by a few productive basins, even if it may have been less diffuse in the Proterozoic than in modern environments.

## 5. Conclusion

Redox proxies indicate that deposition of the Arctic Bay Formation took place in a stratified water column with oxic surface waters, underlain by an intermittently euxinic proximal region, and finally persistently ferruginous deep waters.  $\delta^{15}\text{N}$  values and TOC/TN ratios suggest that the importance of different nitrogen cycle processes, such as ammonia volatilisation, nitrogen fixation, and partial nitrification and denitrification varied across the basin depending on redox conditions. The alkaline conditions interpreted during deposition of the Arctic Bay Formation may have played an important role in the efficient sequestration of highly reactive iron in carbonate minerals, resulting in the sulphurisation of organic matter by 'excess' sulphur. Estimates of organic carbon burial rates during deposition of the Arctic Bay Formation indi-



cate that although this shale succession is highly organic-rich, it may have been the result of efficient organic carbon preservation, aided by dominantly anoxic conditions and sulphurisation of organic matter, rather than extraordinarily high primary productivity – although such a scenario cannot be ruled out. The Monte Carlo results presented here suggest that efficient organic matter burial could occur in Precambrian environments across a wide range of conditions, although redox-stratified intracratonic basins may be loci for elevated organic carbon burial, and the OM burial rates calculated for the Arctic Bay Formation are consistent with modern intracontinental and terrestrial basins, as well as Proterozoic lacustrine basins. Thus, although the very high TOC shales of the Arctic Bay Formation seem inconsistent with the low biological productivity that has been hypothesised throughout much of the Proterozoic, data presented here indicates that even unusually organic-rich black shales may require only moderately elevated organic carbon burial rates, perhaps 5 to 6 times higher than the global average during this time.

### Declaration of competing interest

The authors declare that they have no known competing financial interests or personal relationships that could have appeared to influence the work reported in this paper.

### Acknowledgements

We thank Sarah Wörndle and Vivien M. Cumming for their contributions during fieldwork, and Tessa N. Browne for laboratory assistance. The hamlets of Pond Inlet and Arctic Bay, and the respective Hunters and Trappers Associations, are thanked for their support to conduct this research. Eva Stüeken Lou Derry, and an anonymous reviewer are thanked for their constructive feedback. MSWH acknowledges funding for field work provided by an NSERC USRA and the NSTP. MK acknowledges financial support through scholarships awarded by the Department of Earth & Planetary Sciences, McGill University, and GEOTOP. PWC acknowledges funding through NSTP and an NSERC CREATE CATP Fellowship. EAS acknowledges a Sloan Ocean Sciences Fellowship and the donors of The American Chemical Society Petroleum Research Fund for partial support of this research (61017-ND2). TMG acknowledges funding from the Eric Mountjoy Legacy Fund and the Agouron Geobiology Fellowship. GPH acknowledges funding for fieldwork provided by NSERC and Natural Resources Canada (GEM2 and PCSP).

### Appendix A. Supplementary material

Supplementary material related to this article can be found online at <https://doi.org/10.1016/j.epsl.2020.116384>.

### References

- Ader, M., Thomazo, C., Sansjofre, P., Busigny, V., Papineau, D., Laffont, R., Cartigny, P., Halverson, G.P., 2016. Interpretation of the nitrogen isotopic composition of Precambrian sedimentary rocks: assumptions and perspectives. *Chem. Geol.* 429, 93–110.
- Burdige, D.J., 2007. Preservation of organic matter in marine sediments: controls, mechanisms, and an imbalance in sediment organic carbon budgets? *Chem. Rev.* 107, 467–485.
- Canfield, D.E., 1994. Factors influencing organic carbon preservation in marine sediments. *Chem. Geol.* 114, 315–329.
- Canfield, D.E., Raiswell, R., Westrich, J.T., Reaves, C.M., Berner, R.A., 1986. The use of chromium reduction in the analysis of reduced inorganic sulfur in sediments and shales. *Chem. Geol.* 54, 149–155.
- Canfield, D.E., Zhang, S., Frank, A.B., Wang, X., Wang, H., Su, J., Ye, Y., Frei, R., 2018. Highly fractionated chromium isotopes in Mesoproterozoic-aged shales and atmospheric oxygen. *Nat. Commun.* 9, 11.
- Cole, D.B., Reinhard, C.T., Wang, X., Gueguen, B., Halverson, G.P., Gibson, T., Hodgskiss, M.S., McKenzie, N.R., Lyons, T.W., Planavsky, N.J., 2016. A shale-hosted Cr isotope record of low atmospheric oxygen during the Proterozoic. *Geology* 44, 555–558.
- Cox, G.M., Jarrett, A., Edwards, D., Crockford, P.W., Halverson, G.P., Collins, A.S., Poirier, A., Li, Z.X., 2016. Basin redox and primary productivity within the Mesoproterozoic Roper Seaway. *Chem. Geol.* 440, 101–114.
- Crockford, P.W., Hayles, J.A., Bao, H., Planavsky, N.J., Bekker, A., Fralick, P.W., Halverson, G.P., Bui, T.H., Peng, Y., Wing, B.A., 2018. Triple oxygen isotope evidence for limited mid-Proterozoic primary productivity. *Nature* 559, 613–616.
- Crockford, P.W., Kunzmann, M., Bekker, A., Hayles, J., Bao, H., Halverson, G.P., Peng, Y., Bui, T.H., Cox, G.M., Gibson, T.M., et al., 2019. Claypool continued: extending the isotopic record of sedimentary sulfate. *Chem. Geol.* 513, 200–225.
- Cumming, V.M., Selby, D., Lillis, P.G., 2012. Re–Os geochronology of the lacustrine Green River Formation: insights into direct depositional dating of lacustrine successions, Re–Os systematics and paleocontinental weathering. *Earth Planet. Sci. Lett.* 359, 194–205.
- Derry, L.A., 2015. Causes and consequences of mid-Proterozoic anoxia. *Geophys. Res. Lett.* 42, 8538–8546.
- Diamond, C.W., Planavsky, N.J., Wang, C., Lyons, T.W., 2018. What the ~1.4 Ga Ximaming Formation can and cannot tell us about the mid-Proterozoic ocean. *Geobiology* 16, 219–236.
- Emmings, J.F., Hennissen, J.A., Stephenson, M.H., Poulton, S.W., Vane, C.H., Davies, S.J., Leng, M.J., Lamb, A., Moss-Hayes, V., 2019. Controls on amorphous organic matter type and sulphurization in a Mississippian black shale. *Rev. Palaeobot. Palynol.* 268, 1–18.
- Fustic, M., Ardakani, O.H., Jiang, C., Turner, E.C., Mort, A., Sanei, H., Gonzales, G., Long, D., 2017. Preliminary petroleum potential and organic matter characterization of the Mesoproterozoic upper Arctic Bay Formation (black shale) at the Shale Valley Central, northern Baffin Island, Nunavut, Canada. In: *Subsurface Hydrocarbon Movement, Gussow Research Conference*.
- Gibson, T.M., Shih, P.M., Cumming, V.M., Fischer, W.W., Crockford, P.W., Hodgskiss, M.S., Wörndle, S., Creaser, R.A., Rainbird, R.H., Skulski, T.M., et al., 2018. Precise age of *Bangiomorpha pubescens* dates the origin of eukaryotic photosynthesis. *Geology* 46, 135–138.
- Gibson, T.M., Wörndle, S., Crockford, P.W., Bui, T.H., Creaser, R.A., Halverson, G.P., 2019. Radiogenic isotope chemostratigraphy reveals marine and nonmarine depositional environments in the late Mesoproterozoic Borden Basin, Arctic Canada. *Geol. Soc. Am. Bull.* 131, 1965–1978.
- Gibson, T.M., Kunzmann, M., Poirier, A., Schumann, D., Tosca, N.J., Halverson, G.P., 2020. Geochemical signatures of transgressive shale intervals from the 811 Ma Fifteenmile Group in Yukon, Canada: disentangling sedimentary redox cycling from weathering alteration. *Geochim. Cosmochim. Acta*. <https://doi.org/10.1016/j.gca.2020.04.013>.
- Gilleaudeau, G.J., Kah, L.C., 2015. Heterogeneous redox conditions and a shallow chemocline in the Mesoproterozoic ocean: evidence from carbon–sulfur–iron relationships. *Precambrian Res.* 257, 94–108.
- Gilleaudeau, G.J., Kah, L.C., 2013. Carbon isotope records in a Mesoproterozoic epicratonic sea: carbon cycling in a low-oxygen world. *Precambrian Res.* 228, 85–101.
- Hahn, K.E., Turner, E.C., 2017. Composition and history of giant carbonate seep mounds, Mesoproterozoic Borden Basin, Arctic Canada. *Precambrian Res.* 293, 150–173.
- Hahn, K.E., Turner, E.C., Babechuk, M.G., Kamber, B.S., 2015. Deep-water seep-related carbonate mounds in a Mesoproterozoic alkaline lake, Borden Basin (Nunavut, Canada). *Precambrian Res.* 271, 173–197.
- Hartnett, H.E., Keil, R.G., Hedges, J.L., Devol, A.H., 1998. Influence of oxygen exposure time on organic carbon preservation in continental margin sediments. *Nature* 391 (6667), 572–575.
- Hedges, J.L., Keil, R.G., 1995. Sedimentary organic matter preservation: an assessment and speculative synthesis. *Mar. Chem.* 49, 81–115.
- Hemingway, J.D., Rothman, D.H., Grant, K.E., Rosengard, S.Z., Eglinton, T.I., Derry, L.A., Galy, V.V., 2019. Mineral protection regulates long-term global preservation of natural organic carbon. *Nature* 570, 228–231.
- Hickson, C.J., Juras, S.J., 1986. Sample contamination by grinding. *Can. Mineral.* 24 (3), 585–589.
- Hodgskiss, M.S.W., Kunzmann, M., Poirier, A., Halverson, G.P., 2018. The role of microbial iron reduction in the formation of Proterozoic molar tooth structures. *Earth Planet. Sci. Lett.* 482, 1–11.
- Hodgskiss, M.S.W., Crockford, P.W., Peng, Y., Wing, B.A., Horner, T.J., 2019. A productivity collapse to end Earth's Great Oxidation. *Proc. Natl. Acad. Sci. USA* 116, 17207–17212.
- Horton, F., 2015. Did phosphorus derived from the weathering of large igneous provinces fertilize the Neoproterozoic ocean? *Geochem. Geophys. Geosyst.* 16 (6), 1723–1738.
- Hülse, D., Arndt, S., Ridgwell, A., 2019. Mitigation of extreme Ocean Anoxic Event conditions by organic matter sulfurization. *Paleoceanogr. Paleoclimatol.* 34, 476–489.
- Jackson, G., Ianelli, T., 1981. Rift related cyclic sedimentation in the Neo-Helikian Borden Basin, NW Baffin Island. Geological Survey of Canada Paper, pp. 81–10.
- Jarrett, A.J., Cox, G.M., Brocks, J.J., Grosjean, E., Boreham, C.J., Edwards, D.S., 2019. Microbial assemblage and palaeoenvironmental reconstruction of the 1.38 Ga Velkerri Formation, McArthur Basin, northern Australia. *Geobiology* 17, 360–380.

- Jones, S.M., Prave, A.R., Raub, T.D., Cloutier, J., Stüeken, E.E., Rose, C.V., Linnekogel, S., Nazarov, K., 2020. A marine origin for the late Mesoproterozoic Copper Harbor and Nonesuch Formations of the Midcontinent Rift of Laurentia. *Precambrian Res.* 336, 105510.
- Kah, L.C., Bartley, J.K., Teal, D.A., 2012. Chemostratigraphy of the Late Mesoproterozoic Atar Group, Taoudeni Basin, Mauritania: muted isotopic variability, facies correlation, and global isotopic trends. *Precambrian Res.* 200, 82–103.
- Katsev, S., Crowe, S.A., 2015. Organic carbon burial efficiencies in sediments: the power law of mineralization revisited. *Geology* 43, 607–610.
- Kendall, B., Creaser, R.A., Gordon, G.W., Anbar, A.D., 2009a. Re–Os and Mo isotope systematics of black shales from the Middle Proterozoic Velkerri and Wollongorang formations, McArthur Basin, northern Australia. *Geochim. Cosmochim. Acta* 73 (9), 2534–2558.
- Kendall, B., Creaser, R.A., Selby, D., 2009b.  $^{187}\text{Re}$ – $^{187}\text{Os}$  geochronology of Precambrian organic-rich sedimentary rocks. *Geol. Soc. (Lond.) Spec. Publ.* 326 (1), 85–107.
- Kennedy, M.J., Pevear, D.R., Hill, R.J., 2002. Mineral surface control of organic carbon in black shale. *Science* 295, 657–660.
- Kipp, M.A., Stüeken, E.E., Yun, M., Bekker, A., Buick, R., 2018. Pervasive aerobic nitrogen cycling in the surface ocean across the Paleoproterozoic Era. *Earth Planet. Sci. Lett.* 500, 117–126.
- Kunzmann, M., Gibson, T.M., Halverson, G.P., Hodgskiss, M.S., Bui, T.H., Carozza, D.A., Sperling, E.A., Poirier, A., Cox, G.M., Wing, B.A., 2017. Iron isotope biogeochemistry of Neoproterozoic marine shales. *Geochim. Cosmochim. Acta* 209, 85–105.
- Laakso, T.A., Schrag, D.P., 2014. Regulation of atmospheric oxygen during the Proterozoic. *Earth Planet. Sci. Lett.* 38, 81–91.
- Laakso, T.A., Schrag, D.P., 2018. Limitations on limitation. *Glob. Biogeochem. Cycles* 32, 486–496.
- Laakso, T.A., Schrag, D.P., 2019. A small marine biosphere in the Proterozoic. *Geobiology* 17, 161–171.
- Long, D.G., Turner, E.C., 2012. Tectonic, sedimentary and metallogenic re-evaluation of basal strata in the Mesoproterozoic Bylot basins, Nunavut, Canada: are unconformity-type uranium concentrations a realistic expectation? *Precambrian Res.* 214, 192–209.
- Lyons, T.W., Anbar, A.D., Severmann, S., Scott, C., Gill, B.C., 2009. Tracking euxinia in the ancient ocean: a multiproxy perspective and Proterozoic case study. *Annu. Rev. Earth Planet. Sci.* 37, 507–534.
- Müller, P.J., 1977. CN ratios in Pacific deep-sea sediments: effect of inorganic ammonium and organic nitrogen compounds sorbed by clays. *Geochim. Cosmochim. Acta* 41, 765–776.
- Olson, S.L., Kump, L.R., Kasting, J.F., 2013. Quantifying the areal extent and dissolved oxygen concentrations of Archean oxygen oases. *Chem. Geol.* 362, 35–43.
- Oxburgh, R., 2001. Residence time of osmium in the oceans. *Geochem. Geophys. Geosyst.* 2, 17.
- Ozaki, K., Reinhard, C.T., Tajika, E., 2019. A sluggish mid-Proterozoic biosphere and its effect on Earth's redox balance. *Geobiology* 17, 3–11.
- Peucker-Ehrenbrink, B., Ravizza, G., 2000. The marine osmium isotope record. *Terra Nova* 12, 205–219.
- Planavsky, N.J., Slack, J.F., Cannon, W.F., O'Connell, B., Isson, T.T., Asael, D., Jackson, J.C., Hardisty, D.S., Lyons, T.W., Bekker, A., 2018a. Evidence for episodic oxygenation in a weakly redox-buffered deep mid-Proterozoic ocean. *Chem. Geol.* 483, 581–594.
- Planavsky, N.J., Cole, D.B., Isson, T.T., Reinhard, C.T., Crockford, P.W., Sheldon, N.D., Lyons, T.W., 2018b. A case for low atmospheric oxygen levels during Earth's middle history. *Emerg. Top. Life Sci.* 2, 149–159.
- Poulton, S.W., Canfield, D.E., 2005. Development of a sequential extraction procedure for iron: implications for iron partitioning in continentally derived particulates. *Chem. Geol.* 214, 209–221.
- Raiswell, R., Canfield, D.E., 1998. Sources of iron for pyrite formation in marine sediments. *Am. J. Sci.* 298, 219–245.
- Raiswell, R., Hardisty, D.S., Lyons, T.W., Canfield, D.E., Owens, J.D., Planavsky, N.J., Poulton, S.W., Reinhard, C.T., 2018. The iron paleoredox proxies: a guide to the pitfalls, problems and proper practice. *Am. J. Sci.* 318, 491–526.
- Reinhard, C.T., Planavsky, N.J., Olson, S.L., Lyons, T.W., Erwin, D.H., 2016. Earth's oxygen cycle and the evolution of animal life. *Proc. Natl. Acad. Sci. USA* 113, 8933–8938.
- Rooney, A.D., Selby, D., Houzay, J.-P., Renne, P.R., 2010. Re–Os geochronology of a Mesoproterozoic sedimentary succession, Taoudeni basin, Mauritania: implications for basin-wide correlations and Re–Os organic-rich sediments systematics. *Earth Planet. Sci. Lett.* 289, 486–496.
- Rooney, A.D., Selby, D., Lloyd, J.M., Roberts, D.H., Lückge, A., Sageman, B.B., Prouty, N.G., 2016. Tracking millennial-scale Holocene glacial advance and retreat using osmium isotopes: insights from the Greenland ice sheet. *Quat. Sci. Rev.* 138, 49–61.
- Scott, C., Lyons, T.W., 2012. Contrasting molybdenum cycling and isotopic properties in euxinic versus non-euxinic sediments and sedimentary rocks: refining the paleoproxies. *Chem. Geol.* 324, 19–27.
- Sherman, A.G., James, N.P., Narbonne, G.M., 2002. Evidence for reversal of basin polarity during carbonate ramp development in the Mesoproterozoic Borden Basin, Baffin Island. *Can. J. Earth Sci.* 39 (4), 519–538.
- Sperling, E.A., Carbone, C., Strauss, J.V., Johnston, D.T., Narbonne, G.M., Macdonald, F.A., 2016. Oxygen, facies, and secular controls on the appearance of Cryogenian and Ediacaran body and trace fossils in the Mackenzie Mountains of northwestern Canada. *Geol. Soc. Am. Bull.* 128, 558–575.
- Sperling, E.A., Halverson, G.P., Knoll, A.H., Macdonald, F.A., Johnston, D.T., 2013. A basin redox transect at the dawn of animal life. *Earth Planet. Sci. Lett.* 371, 143–155.
- Spinks, S.C., Parnell, J., Bowden, S.A., Taylor, R.A., Maclean, M.E., 2014. Enhanced organic carbon burial in large Proterozoic lakes: implications for atmospheric oxygenation. *Precambrian Res.* 255, 202–215.
- Stüeken, E.E., 2013. A test of the nitrogen-limitation hypothesis for retarded eukaryote radiation: nitrogen isotopes across a Mesoproterozoic basinal profile. *Geochim. Cosmochim. Acta* 120, 121–139.
- Stüeken, E.E., Martinez, A., Love, G., Olsen, P.E., Bates, S., Lyons, T.W., 2019. Effects of pH on redox proxies in a Jurassic rift lake: implications for interpreting environmental records in deep time. *Geochim. Cosmochim. Acta* 252, 240–267.
- Stüeken, E.E., Tino, C., Arp, G., Jung, D., Lyons, T.W., 2020. Nitrogen isotope ratios trace high-pH conditions in a terrestrial Mars analog site. *Sci. Adv.* 6 (9), eaay3440.
- Reinhard, C.T., Planavsky, N.J., Gill, B.C., Ozaki, K., Robbins, L.J., Lyons, T.W., Fischer, W.W., Wang, C., Cole, D.B., Konhauser, K.O., 2017. Evolution of the global phosphorus cycle. *Nature* 541, 386–389.
- Tosca, N.J., Johnston, D.T., Mushegian, A., Rothman, D.H., Summons, R.E., Knoll, A.H., 2010. Clay mineralogy, organic carbon burial, and redox evolution in Proterozoic oceans. *Geochim. Cosmochim. Acta* 74, 1579–1592.
- Turner, E.C., 2009. Mesoproterozoic carbonate systems in the Borden Basin, Nunavut. *Can. J. Earth Sci.* 46, 915–938.
- Turner, E.C., Kamber, B.S., 2012. Arctic Bay Formation, Borden Basin, Nunavut (Canada): basin evolution, black shale, and dissolved metal systematics in the Mesoproterozoic ocean. *Precambrian Res.* 208, 1–18.
- Tuttle, M.L., Rice, C.A., Goldhaber, M.B., 1990. Case studies of freshwater and saline lakes. In: *Geochemistry of Organic and Inorganic Sulfur in Ancient and Modern Lacustrine Environments*.
- Tuttle, M.L., Goldhaber, M.B., 1993. Sedimentary sulfur geochemistry of the Paleogene Green River Formation, western USA: implications for interpreting depositional and diagenetic processes in saline alkaline lakes. *Geochim. Cosmochim. Acta* 57, 3023–3039.
- Vallina, S.M., Follows, M., Dutkiewicz, S., Montoya, J.M., Cermeno, P., Loreau, M., 2014. Global relationship between phytoplankton diversity and productivity in the ocean. *Nat. Commun.* 5, 4299.
- Walsh, J.J., 1991. Importance of continental margins in the marine biogeochemical cycling of carbon and nitrogen. *Nature* 350, 53.
- Wedepohl, K.H., 1995. The composition of the continental crust. *Geochim. Cosmochim. Acta* 59, 1217–1232.
- Werne, J.P., Hollander, D.J., Lyons, T.W., Sinninghe Damsté, J.S., 2004. Organic sulfur biogeochemistry: recent advances and future research directions. *Spec. Pap., Geol. Soc. Am.*, 135–150.
- Zhang, S., Wang, X., Wang, H., Bjerrum, C.J., Hammarlund, E.U., Costa, M.M., Connelly, J.N., Zhang, B., Su, J., Canfield, D.E., 2016. Sufficient oxygen for animal respiration 1,400 million years ago. *Proc. Natl. Acad. Sci. USA* 113, 1731–1736.
- Zimmerman, A.R., Canuel, E.A., 2000. A geochemical record of eutrophication and anoxia in Chesapeake Bay sediments: anthropogenic influence on organic matter composition. *Mar. Chem.* 69 (1–2), 117–137.